

A methodological comparison of interaction neighborhoods in the social force model of panic evacuation

Wenhan Wu ^a, Wenfeng Yi ^{b,*}

^a Senseable City Laboratory, Massachusetts Institute of Technology, Cambridge, MA, 02139, USA

^b College of Artificial Intelligence, China University of Petroleum, 102249, Beijing, China

ARTICLE INFO

Keywords:

Interaction neighborhood
Crowd behavior
Escape panic
Decision-making
Evacuation dynamics

ABSTRACT

Crowd evacuation exhibits diverse behavioral patterns from individualistic to herding, depending on the degree of panic. These patterns essentially arise from social interactions between individuals, however, how different neighborhood hypotheses affect crowd dynamics in panic evacuation remains unclear. Here, we adopt a social force model of escape panic, where interaction neighborhoods are defined by metric, topological, or visual networks. Numerical simulations show that all three neighborhood definitions reproduce the individualistic-to-herding transition, while shaping individual decisions and collective outcomes differently. Each interaction rule uniquely characterizes the proportion of effective neighbors, with larger neighborhood scales generally increasing exit usage asymmetry and slowing evacuation. Visual neighborhoods outperform metric and topological ones, as occlusion-induced constraints provide robust adaptivity and capture realistic, density-geometry dependent decision dynamics. At higher panic, leaving time becomes more polarized across density levels and neighborhood scales, with its minimum value largely independent of neighborhood definitions. Finally, we identify optimal regimes of decision-making rationality as stronger herding in sparse or small-neighborhood cases, greater individualism in dense and large-neighborhood ones, and intermediate strategy otherwise. This study highlights the sensitivity of evacuation predictions to neighborhood assumptions within the modeling framework, and provides a methodological benchmark for selecting interaction rules in simulation-based evacuation analysis.

1. Introduction

As crowd-related incidents gradually increase in scale and frequency [1,2], understanding human behavior during emergencies has become a critical issue in public security and urban management [3]. The decision-making and movement of individuals play a core role in crowd evacuation [4,5], collectively determining evacuation efficiency and safety outcomes. With rapid advances in computer science, computational modeling has attracted considerable interest for simulating complex crowd dynamics and evaluating evacuation strategies across various scenarios [6,7]. These insights, derived from numerical simulations, are valuable not only for analyzing and predicting human behavior, but also for designing safety measures that can potentially save more lives [8,9].

One of the most typical crowd behaviors in human crowds is herding behavior [10], which refers to people resorting to the decisions made by others as additional sources of information to improve their own decisions and imitate the actions of their neighbors [11]. This phenomenon often occurs when there is a certain degree of uncer-

tainty in the decision-making context [12], such as the choice of direction (or exit) during emergency evacuation. In such situations, escape panic will intensify if accompanied by time pressure or limited visibility, thereby further amplifying the tendency to follow others [13]. The current progress in herding behavior in emergency evacuation can be divided into two aspects according to research methods. In terms of controlled experiments, internal individual factors (e.g., personality traits [14] and exit familiarity [15]) and external environmental factors (e.g., smoke level [16], direction signs [17], and crowd density [18]) have been confirmed to influence herding behavior and evacuation decisions. A virtual experiment demonstrated that one is more likely to leave if this person sees more people leaving [19], while another crowd experiment claimed the opposite conclusion that humans do not tend to imitate the direction choices of the majority [20]. While experimental studies can qualitatively reveal the laws or patterns of herding behavior, computational modeling has become another crucial means for a deeper quantitative understanding of its underlying mechanisms. Recently, researchers have proposed a discrete choice model based on random utilities [21,22], a utility threshold model based on complex network

* Corresponding author.

E-mail addresses: wenhanwu@mit.edu (W. Wu), wenfengyi@cup.edu.cn (W. Yi).

theory [23], and a parametric model of decision-making [11] to explore the impacts of herding behavior on exit choice and crowd evacuation. The most widely known and used is the social force model [24], this pioneering work utilized a panic parameter to reproduce the herding behavior, where individuals may either select an individual direction or follow the average direction of neighbors, or try a mixture of both. Nevertheless, a critical question still remains: what are the rules that determine the neighbors with which an individual interacts? In Helbing et al.'s work [24] and many subsequent extensions [25–27], the interaction neighborhood was defined via a metric hypothesis by default, without explicitly considering the consequences of alternative neighborhood definitions. To our knowledge, no prior study has systematically compared different interaction hypotheses within a unified collective human motion model, nor investigated their impacts on crowd behavior during the evacuation process.

Existing studies on mathematical models of collective motion typically classify the interaction neighborhood into three categories: metric, topological, and visual [28]. The metric neighborhood assumes that all individuals within a zone of fixed radius are potential neighbors, and the interaction strength generally decays with metric distance. This hypothesis has been widely confirmed in collective motion studies of animal groups and human crowds [29–31]. In contrast, the topological neighborhood defines neighbors not by absolute physical distance, but by the rank order of relative distance (i.e., a fixed number of nearest neighbors), with neighbor influence decreasing with ordinal rank. This concept has been confirmed by empirical observations in animal groups such as bird flocks [32,33], and also in controlled human experiments [34]. Yet the two hypotheses both ignore sensory information by relying on specific rules, which limits their ability to accurately capture the social cues available to individuals [35]. Recently, the visual neighborhood has been proposed, emphasizing that interactions are constrained by the field of view and visual occlusion. This definition aligns closely with cognitive processes in reality, where neighbors depend primarily on what individuals see rather than purely on distance or rank [36]. The visual neighborhood has been demonstrated to outperform metric and topological ones in explaining the collective motion of both fish schools and human crowds [37,38]. Despite these advances, existing comparisons of these interaction neighborhoods have been conducted mainly in animal groups and in controlled human experiments under normal conditions, while their explicit and systematic comparisons in panic evacuation scenarios remain limited. Emergency evacuation involves heightened uncertainty, time pressure, and spatial constraints, under which interaction rules validated in non-panic settings may produce distinct collective responses. In particular, how different interaction neighborhoods shape effective coupling structures, collective escape patterns and evacuation performance across varying panic degrees, density levels and neighborhood scales has not yet been fully explored. Therefore, addressing this research question is essential for clarifying the role of interaction assumptions in panic escape and for improving our understanding of crowd behavior in emergency situations.

In this work, we adopt a social force model of escape panic and systematically extend it by incorporating different definitions of interaction neighborhoods to study crowd behavior during emergency evacuation. Specifically, three typical interaction networks are considered: metric networks determined by a fixed distance range, topological networks defined by the number of nearest neighbors, and visual networks characterized by the angular area occupied in the visual field. Based on this framework, a series of numerical simulations are systematically conducted: First, we qualitatively and quantitatively analyze crowd behavior in panic evacuation and find that neighborhood hypotheses may have different degrees of influence on individual decisions and collective outcomes. Then, the average proportion of neighbors, the absolute difference in exit usage, and the leaving time for 90 % people are adopted to investigate the effects of interaction neighborhoods on panic evacuation. Finally, we examine the leaving time under different evacuation conditions (panic degree, density level, and neighborhood scale), and

summarize optimal regimes of decision-making rationality for efficient evacuation. These results are intended to provide a methodological comparison of interaction neighborhoods in panic evacuation and to clarify how varying neighborhood definitions influence the numerical sensitivity of evacuation predictions.

The rest of this paper is organized as follows. Section 2 describes a mathematical model with different neighborhood definitions. Section 3 conducts numerical simulations to analyze how interaction neighborhoods affect crowd behavior in panic evacuation. Finally, relevant conclusions and discussions are presented in Section 4.

2. Methods

2.1. Definitions of interaction neighborhoods

We use metric, topological, and visual networks to define different types of interaction neighborhoods (as shown in Fig. 1), to which the individuals belonging have edges connected to the focal individual. In general, the adjacency matrix A contains information for each pair of individuals i and j about whether they are connected, where $A_{ij} = 1$ if a link from i to j exists, and $A_{ij} = 0$ otherwise. The rules for determining the existence of links are provided based on the following network types.

2.1.1. Metric networks

Metric networks are the most common framework for describing the local interaction range and serve as the foundation for many collective motion models. In such networks, the existence of a connection between individuals depends solely on their Euclidean distance $d_{ij} = \|\mathbf{x}_i - \mathbf{x}_j\|$, where \mathbf{x}_i and \mathbf{x}_j are the positions of individuals i and j . Specifically, two individuals are linked if their distance d_{ij} is smaller than a metric threshold R_{metr} :

$$A_{ij}^{\text{metr}} = \begin{cases} 1, & d_{ij} \leq R_{\text{metr}} \\ 0, & d_{ij} > R_{\text{metr}} \end{cases} \quad (1)$$

This rule is illustrated in Fig. 1(a), where all individuals located within a radius of R_{metr} form incoming links with the focal individual j , and a link between individuals i and j is not influenced by the positions of other individuals. Given that Euclidean distance is symmetric ($d_{ij} = d_{ji}$), metric networks are therefore undirected by nature.

2.1.2. Topological networks

Topological (also known as the k-nearest neighbors) networks are a widely recognized candidate for describing local interactions and have recently received empirical support in studies of collective human behavior [34]. In such networks, the existence of a connection between individuals relies on the spatial arrangement of all other individuals. To formalize this, each individual i is assigned a closeness rank c_{ij} , with respect to individual j as $c_{ij} = |\{m | d_{mj} < d_{ij}\}| + 1$, where $|\cdot|$ represents the cardinality of the set. Here, a fixed number N_{topo} of nearest neighbors is connected to the focal individual j :

$$A_{ij}^{\text{topo}} = \begin{cases} 1, & c_{ij} \leq N_{\text{topo}} \\ 0, & c_{ij} > N_{\text{topo}} \end{cases} \quad (2)$$

The corresponding rule is shown in Fig. 1(b), where the incoming links are determined by ranking all others according to their Euclidean distance to individual j . Topological networks are typically directed because the closeness rank is not necessarily reciprocal. Note that we adopt the fraction of nearest neighbors $\eta_{\text{topo}} = N_{\text{topo}}/N$ as a topological threshold to facilitate comparability across different population sizes.

2.1.3. Visual networks

In recent years, visual networks have attracted considerable attention because the cognitive mechanisms of social interactions can be well reflected. In such networks, the existence of a connection between individuals is based on their visual perception of each other. Here, a link

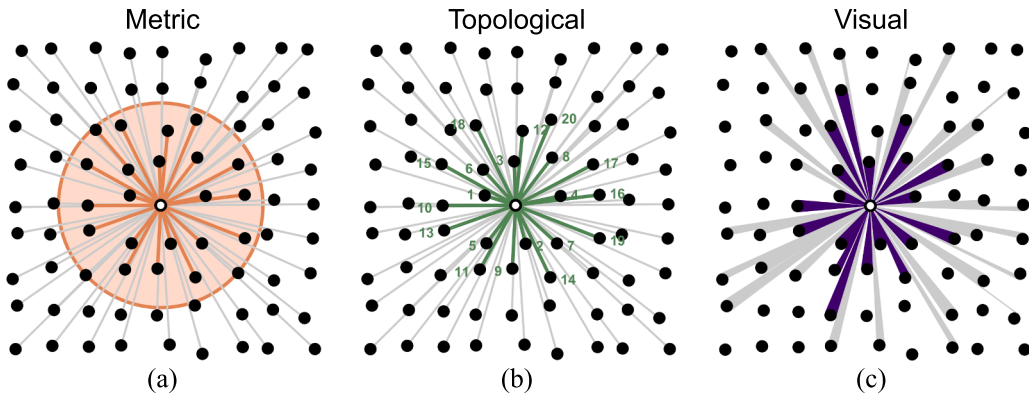


Fig. 1. Illustration of interaction neighborhoods defined by different network types. (a) Metric network. (b) Topological network. (c) Visual network. The neighbors of the focal individual (hollow circle) are connected by orange lines, green lines, and purple visual fields, respectively.

from individual i to j can be established if i is visible to j . That is, the angular area α_{ij} (i.e., the angle that the visible part of individual i occupies in the visual field of j) exceeds a visual threshold θ_{vis} :

$$A_{ij}^{\text{vis}} = \begin{cases} 1, & \alpha_{ij} > \theta_{\text{vis}} \\ 0, & \alpha_{ij} \leq \theta_{\text{vis}} \end{cases} \quad (3)$$

The rule in Fig. 1(c) can be easily understood to determine the interaction neighborhood. Additionally, θ_{vis} applies to the visible portion if individual i is partially occluded by others. The determination of $\alpha_{ij} \left(\leq \alpha_{ij}^{\text{free}} \right)$ follows by first calculating the unobstructed visual angle $\alpha_{ij}^{\text{free}}$ of i in the visual field of j , and then subtracting the obstructed portion identified by numerical ray casting at angles specified by the analytics (for further aspects see Ref. [28]). Due to the potential asymmetry of visibility, visual networks are usually directed.

Compared with metric and topological networks, visual networks require additional geometric computations to process occlusion effects, including numerical ray casting and angular subtraction. Although this introduces higher theoretical computational overhead, the associated cost is inherently localized and geometry-bounded. Occlusion handling is restricted to pedestrians within the visual field and primarily involves nearby individuals, thus the effective number of interacting individuals remains limited even in dense environments. As a result, the practical computational cost of visual networks remains scalable and does not grow super-linearly with the size of the crowd or environment.

2.2. Equations of pedestrian movement

The social force model [24] that describes the dynamical features of escape panic is employed to simulate pedestrian movement. In this study, the model is parametrically extended through the above definitions of interaction neighborhoods, which are used for calculating the average direction of neighbors.

The position $\mathbf{x}_i(t)$ of pedestrian i is updated by:

$$\frac{d\mathbf{x}_i(t)}{dt} = \mathbf{v}_i(t) \quad (4)$$

where the change of velocity $\mathbf{v}_i(t)$ is governed by the following acceleration equation:

$$m_i \frac{d\mathbf{v}_i(t)}{dt} = \mathbf{f}_{id} + \sum_{j(\neq i)} \mathbf{f}_{ij} + \sum_W \mathbf{f}_{iW} \quad (5)$$

The first term \mathbf{f}_{id} represents a self-driven force that propels pedestrians toward the destination:

$$\mathbf{f}_{id} = m_i \frac{v_i^0(t)\mathbf{e}_i^0(t) - \mathbf{v}_i(t)}{\tau_i} \quad (6)$$

where pedestrian i of mass m_i tends to adapt his/her actual velocity $\mathbf{v}_i(t)$ within a characteristic time τ_i , so as to move with a desired speed $v_i^0(t)$

in a desired direction $\mathbf{e}_i^0(t)$:

$$\mathbf{e}_i^0(t) = \frac{(1-p_i)\mathbf{e}_i + p_i \langle \mathbf{e}_q^0(t) \rangle_i}{\| (1-p_i)\mathbf{e}_i + p_i \langle \mathbf{e}_q^0(t) \rangle_i \|} \quad (7)$$

where the panic parameter p_i is treated as a linear weighting factor between an individual desired direction \mathbf{e}_i and the average direction $\langle \mathbf{e}_q^0(t) \rangle_i$ of neighbors q (determined by metric, topological, or visual network). Given that the concept of panic itself lacks a unified empirical definition in the evacuation literature [39], p_i is introduced as an abstract behavioral proxy capturing the reliance on social cues and imitative behavior under emergency uncertainty. We acknowledge that such a single scalar parameter cannot capture the multidimensional and context-dependent nature of panic-related behaviors, but it provides a simple formulation that is sufficient for isolating the effects of different interaction neighborhoods.

The second term \mathbf{f}_{ij} accounts for interactions with other pedestrians j :

$$\mathbf{f}_{ij} = A_i \exp [(r_{ij} - d_{ij})/B_i] \mathbf{n}_{ij} + kg(r_{ij} - d_{ij}) \mathbf{n}_{ij} + \kappa g(r_{ij} - d_{ij}) \Delta v_{ji}^t \mathbf{t}_{ij} \quad (8)$$

Here, the psychological tendency of pedestrians i and j to stay away from each other is described by a repulsive interaction force $A_i \exp [(r_{ij} - d_{ij})/B_i] \mathbf{n}_{ij}$, where A_i and B_i are constants, r_{ij} is the sum of their radii r_i and r_j , and \mathbf{n}_{ij} denotes the normalized vector pointing from pedestrian j to i . Two additional forces, a body force $kg(r_{ij} - d_{ij}) \mathbf{n}_{ij}$ and a sliding friction force $\kappa g(r_{ij} - d_{ij}) \Delta v_{ji}^t \mathbf{t}_{ij}$, are introduced to counteract body compression and impede relative tangential motion, respectively. The parameters k and κ reflect the obstruction effects caused by physical contact, $\mathbf{t}_{ij} = (-n_{ij}^2, n_{ij}^1)$ is the tangential direction, and $\Delta v_{ji}^t = (\mathbf{v}_j - \mathbf{v}_i) \cdot \mathbf{t}_{ij}$ is the tangential velocity difference. The function $g(x)$ is zero if pedestrians i and j do not touch each other, otherwise it equals the argument x .

Analogously, the final term \mathbf{f}_{iW} considers interactions between pedestrian i and wall W :

$$\mathbf{f}_{iW} = A_i \exp [(r_i - d_{iW})/B_i] \mathbf{n}_{iW} + kg(r_i - d_{iW}) \mathbf{n}_{iW} - \kappa g(r_i - d_{iW})(\mathbf{v}_i \cdot \mathbf{t}_{iW}) \mathbf{t}_{iW} \quad (9)$$

In this case, d_{iW} is the distance to wall W , with \mathbf{n}_{iW} as the direction perpendicular to it, and \mathbf{t}_{iW} as the direction tangential to it.

3. Numerical simulations

3.1. Experiment setup

To simulate crowd behavior in panic evacuation, we design a smoky square room with static visibility conditions, as shown in Fig. 2. The size

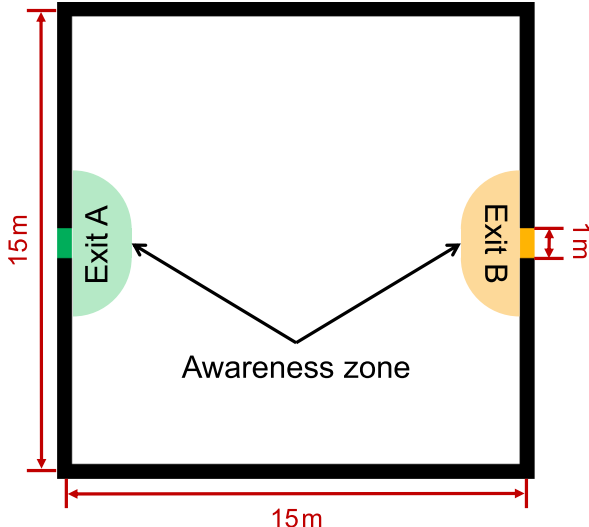


Fig. 2. Schematic diagram of the smoky square room. The black bars around the room denote walls, while green and orange strips represent Exit A and Exit B, with the surrounding light-colored areas denoting the awareness zone.

of this room is $15\text{ m} \times 15\text{ m}$, enclosed by black solid walls. The room is equipped with two available exits: Exit A (green strip) positioned on the left wall and Exit B (orange strip) on the right wall, both with a width of 1 m . At the initial time, pedestrians are uniformly distributed in the room and choose their desired directions randomly. Afterwards, their movement directions are affected by the average direction of neighbors (responding instantaneously), with the strength of influence depending on the degree of panic. Upon reaching a wall boundary, the movement direction is reflected accordingly. If pedestrians enter the awareness zone (light green or light orange area) within 2 m of an exit, their desired directions will be adjusted toward the nearest exit (i.e., pedestrians are aware of the exit location).

Regarding parameter settings, pedestrians are assumed to be homogeneous in physical and behavioral parameters for simplicity. The values of most parameters in the proposed model are referenced from Ref. [24], including the initial desired speed $v_i^0 = 5\text{ ms}^{-1}$, pedestrian mass $m_i = 80\text{ kg}$, characteristic time $\tau_i = 0.5\text{ s}$, pedestrian radius $r_i = 0.25\text{ m}$, constant parameters $A_i = 2 \cdot 10^3\text{ N}$ and $B_i = 0.08\text{ m}$, body elasticity coefficient $k = 1.2 \cdot 10^5\text{ kg s}^{-2}$, and sliding friction coefficient $\kappa = 2.4 \cdot 10^5\text{ kg m}^{-1}\text{ s}^{-1}$. In addition to parameters with fixed values, the following parameters have been varied in our simulations: initial number of people N , panic parameter p_i , metric threshold R_{metr} , topological threshold η_{topo} , and visual threshold θ_{vis} . It should be emphasized that panic is not a controllable or adaptive variable in the model, which means that pedestrians do not dynamically adjust their panic levels during evacuation. The symbol, description, and value of these parameters are summarized in Table 1. Note that all subsequent simulation results are averaged over 50 independent trials for each parameter combination to ensure statistical robustness.

3.2. Analysis of crowd behavior in panic evacuation

The first goal of our simulations is to analyze emergent crowd behavior in panic evacuation. Initially, the total number of people in the room is set to $N = 100$. For illustrative purposes, metric, topological, and visual networks are assigned representative thresholds $R_{\text{metr}} = 5\text{ m}$, $\eta_{\text{topo}} = 20\%$, and $\theta_{\text{vis}} = 0.05\text{ rad}$, while the panic parameter p_i is set to 0.1, 0.5, and 0.9 to characterize low, medium, and high panic levels. Fig. 3 displays snapshots of panic evacuation with 75% people remaining in the room. At low panic ($p_i = 0.1$), people exhibit predominantly individualistic searching behavior, maintaining a relatively sparse spatial distribution and dispersing toward both exits in relatively balanced pro-

Table 1
Parameter settings of the proposed model.

Symbol	Description	Value
v_i^0	Initial desired speed	5 ms^{-1}
m_i	Pedestrian mass	80 kg
τ_i	Characteristic time	0.5 s
r_i	Pedestrian radius	0.25 m
A_i	Constant 1	$2 \cdot 10^3\text{ N}$
B_i	Constant 2	0.08 m
k	Body elasticity coefficient	$1.2 \cdot 10^5\text{ kg s}^{-2}$
κ	Sliding friction coefficient	$2.4 \cdot 10^5\text{ kg m}^{-1}\text{ s}^{-1}$
N	Initial number of people	Varied
p_i	Panic parameter	Varied
R_{metr}	Metric threshold	Varied
η_{topo}	Topological threshold	Varied
θ_{vis}	Visual threshold	Varied

portions. At medium panic ($p_i = 0.5$), individuals adopt a mixed strategy between rational decision-making and following others, leading to obvious aggregation toward both exits, with slight asymmetry in exit usage but no significant difference. At high panic ($p_i = 0.9$), a strong herding effect drives individuals to follow the behavior of their neighbors, which often results in symmetry breaking [40,41] (i.e., visible congestion occurs at one exit, while the other remains underutilized), without any explicit exit preference or pre-set coordination encoded in the model. Overall, these snapshots visually illustrate the spatial patterns associated with the behavioral transition from individualistic to herding as the panic parameter p_i increases, in good agreement with empirical findings [13,18].

To move beyond a qualitative understanding of crowd behavior in panic evacuation, we create low ($N = 50$), medium ($N = 100$), and high ($N = 150$) density levels by initially setting different numbers of people in the room, and adopt two evaluation metrics here: 1) absolute difference in exit usage, which quantifies the imbalance degree in the number of people leaving through the two exits; 2) leaving time for 90% people, which captures a typical time required by the majority to exit while excluding extreme delays by a few stragglers. Fig. 4 shows the quantitative analysis of panic evacuation under different panic and density levels. It can be seen from Fig. 4(a)–(c) that an increase in panic level leads to a marked growth in exit usage asymmetry, in line with the qualitative pattern observed in Fig. 3. As density increases, this asymmetry becomes evident only at larger p_i (in gray), because intensified spatial constraints strengthen the collective balancing effect, thereby requiring stronger panic to disrupt this stability. The optimal evacuation efficiency in Fig. 4(d)–(f) corresponds to a certain mixture of individualistic and herding behavior at each density level. Interestingly, the optimal region (in gray) of the panic parameter shifts toward lower values with increasing density, because stronger herding reduces the time cost of exit exploration at low density, whereas stronger individualism distributes flow and alleviates overcrowding at high density. These results not only reproduce the well-known findings of Helbing et al.'s simulations [24], but also demonstrate the dependence of evacuation dynamics on crowd density [13].

Although the above simulations confirm that all three interaction neighborhoods are able to characterize dynamical features of crowd behavior in panic evacuation, further inspection of Figs. 3 and 4 reveals that metric, topological, and visual networks differ in how they shape individual decisions and produce collective outcomes. For instance, as shown in Fig. 3, symmetry breaking caused by high panic ($p_i = 0.9$) drives the crowd to gather at a single exit, with the visual network retaining a relatively compact arch, the topological network forming a progressively elongated arch, and the metric network producing the widest lateral spread. This reflects how interaction rules shape arching patterns of crowd gathering: the visual rule with fewer distant visible neighbors limits local interactions to a tighter coordination range, whereas the metric rule with more fixed-range neighbors amplifies

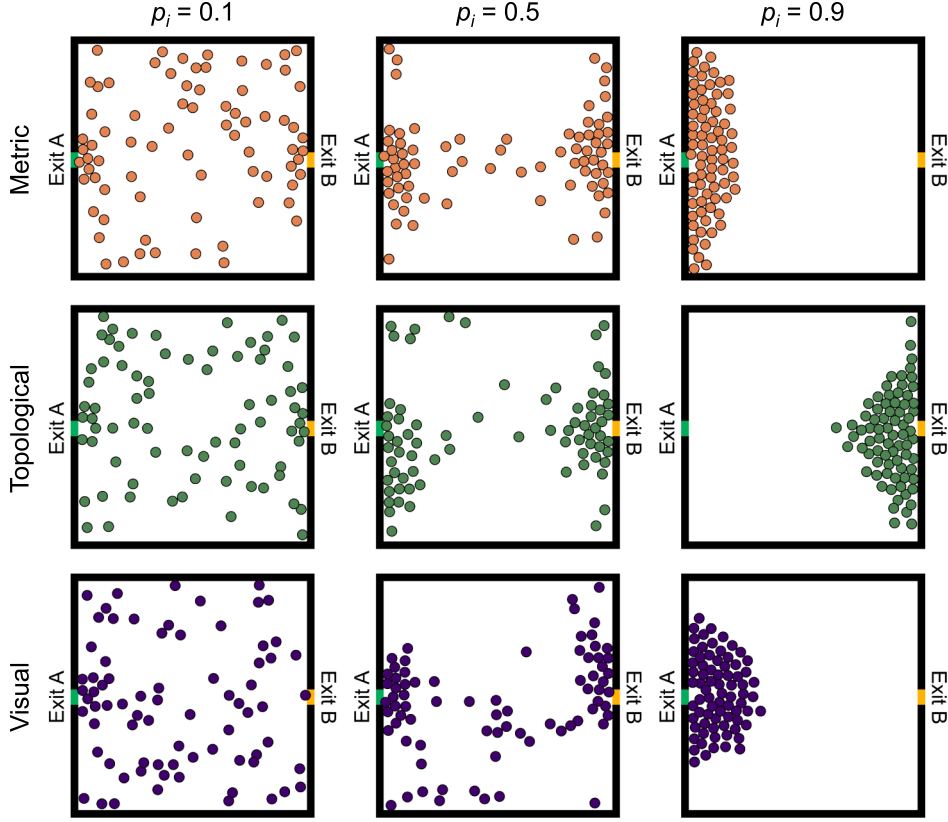


Fig. 3. Snapshots of panic evacuation with 75 % people remaining in the room. From top to bottom are metric, topological, and visual networks, and from left to right are different panic parameters $p_i = 0.1, 0.5$, and 0.9. The individuals are represented by solid circles with different colors.

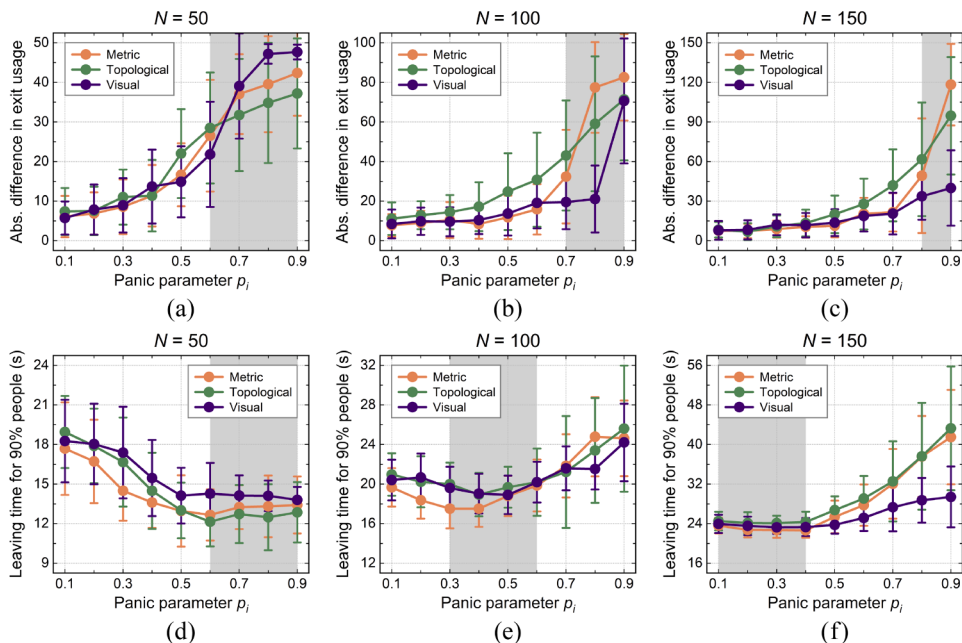


Fig. 4. Quantitative analysis of panic evacuation under different panic and density levels. (a)-(c) Absolute difference in exit usage as a function of panic parameter p_i at low, medium, and high densities. (d)-(f) Leaving time for 90 % people as a function of panic parameter p_i at low, medium, and high densities. The solid circle and error bar represent the mean value and standard deviation in 50 trials, respectively.

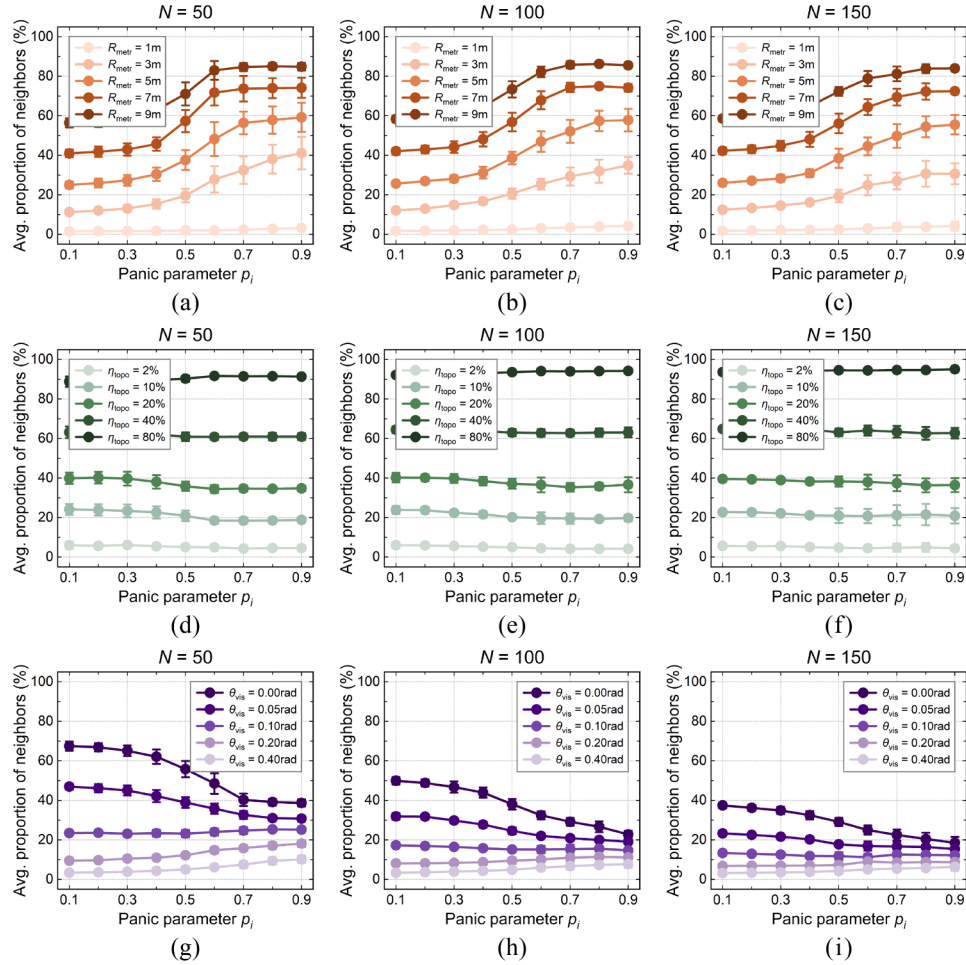


Fig. 5. Effect of interaction neighborhoods on the average proportion of neighbors under different panic and density levels. (a)–(c) Metric network. (d)–(f) Topological network. (g)–(i) Visual network. The solid circle and error bar represent the mean value and standard deviation in 50 trials, respectively.

lateral interactions and outward spreading, and the topological rule balances these extremes by fixing the number of influential neighbors. Moreover, Fig. 4 suggests that density modulates these networks in characteristic ways: at high panic, increasing density reduces asymmetry in exit usage most markedly for visual networks, which in turn improves evacuation efficiency. This is because high density produces more severe visual occlusion, and therefore, the weakening of social influence suppresses collective following, while metric and topological networks are less affected as individuals still maintain a relatively adequate set of neighbors defined by distance or rank. These differences underscore that, although the overarching findings are robust across distinct hypotheses, the mechanisms of information propagation and movement coordination vary in nontrivial ways, making the choice of interaction rules a crucial factor in collective dynamics. This motivates the next section, where we systematically examine how alternative definitions of interaction neighborhoods influence panic evacuation.

3.3. Effects of interaction neighborhoods on panic evacuation

In this section, we are interested in exploring the effects of interaction neighborhoods on panic evacuation. To traverse neighborhood scales from short-range to long-range, three sets of systematic thresholds are varied for metric networks as $R_{\text{metr}} = 1\text{ m}, 3\text{ m}, 5\text{ m}, 7\text{ m}$, and 9 m , for topological networks as $\eta_{\text{topo}} = 2\%, 10\%, 20\%, 40\%$, and 80% , and for visual networks as $\theta_{\text{vis}} = 0.00\text{ rad}, 0.05\text{ rad}, 0.10\text{ rad}, 0.20\text{ rad}$, and 0.40 rad . First, the average proportion of neighbors $\langle N_i^{\text{nei}}(t)/N_{\text{rem}}(t) \rangle_{i,t}$ is defined to measure the effective interaction scale, where $N_i^{\text{nei}}(t)$ and

$N_{\text{rem}}(t)$ are the number of neighbors of individual i and the number of remaining people at time t , respectively. Fig. 5 presents how this measure is affected by interaction neighborhoods under different panic and density levels. For metric networks, as illustrated in Fig. 5(a)–(c), the proportion increases with both R_{metr} and p_i . Enlarging the interaction range spatially captures more neighbors while stronger herding concentrates individuals more quickly, thus larger metric disks accelerate saturation under higher panic conditions. For topological networks, the proportion rises with η_{topo} but remains essentially flat across varying p_i in Fig. 5(d)–(f), because this measure is roughly proportional to the number of nearest neighbors, and the spatial concentration induced by growing panic levels does not significantly affect the curves. For visual networks, as θ_{vis} rises from low to high in Fig. 5(g)–(i), the proportion gradually shifts from decreasing to increasing with p_i . This pattern arises because growing panic leads to higher crowding, which expands the angular area of nearby individuals but reduces the probability of seeing farther neighbors. In terms of density change, the proportion remains almost unchanged for metric networks, as the increase in fixed-range neighbors is offset by normalization over more remaining people. A similar stability is observed for topological networks, since the fraction of nearest neighbors is fixed relative to the initial number of people. In contrast, for visual networks, this measure generally declines at high density due to more pronounced occlusion, which restricts interactions with distant individuals.

How the absolute difference in exit usage varies with interaction neighborhoods under different panic and density levels is analyzed in Fig. 6. A consistent pattern across all panels is that increasing p_i

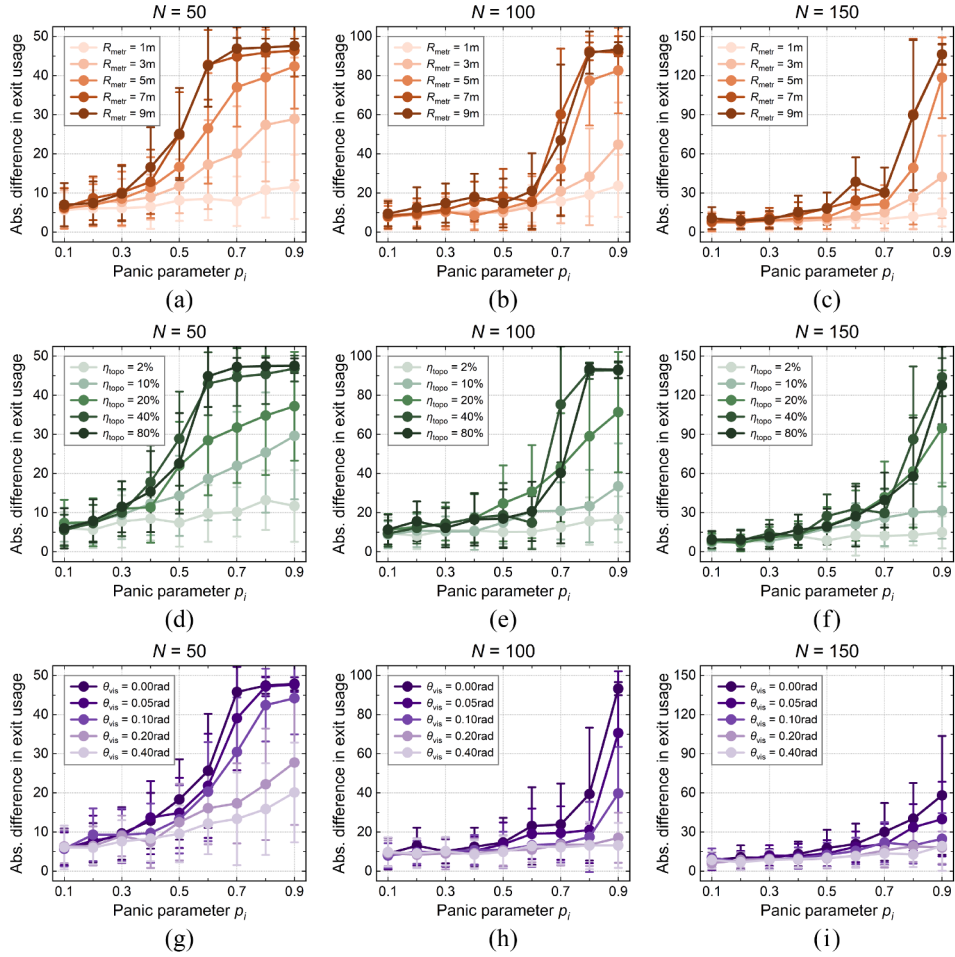


Fig. 6. Effect of interaction neighborhoods on the absolute difference in exit usage under different panic and density levels. (a)–(c) Metric network. (d)–(f) Topological network. (g)–(i) Visual network. The solid circle and error bar represent the mean value and standard deviation in 50 trials, respectively.

produces a marked rise in exit usage imbalance, further amplified by larger R_{metr} , higher η_{topo} , and smaller θ_{vis} , with this effect becoming particularly pronounced at high panic. For metric networks in Fig. 6(a)–(c), larger R_{metr} expands the spatial range and allows individuals to capture more fixed-range neighbors, which strengthens herding dynamics and promotes coherent alignment toward one exit. For topological networks in Fig. 6(d)–(f), increasing η_{topo} adds social links irrespective of physical distance, the amplification is therefore driven by stronger social averaging rather than extending spatial sensing. For visual networks in Fig. 6(g)–(i), lower θ_{vis} makes the visibility criterion easier to satisfy and raises interactions with distant neighbors, thereby speeding the amplification of tiny initial biases into larger symmetry breaking. Notably, higher density makes the curves concave toward the lower right, shifting the inflection point (onset of clear imbalance) to higher p_i regimes and steepening the jump to large asymmetry. Because denser crowds average out small random fluctuations by raising neighbor counts and fostering competing local clusters, thus requiring stronger panic to synchronize collective motion. We also find that, as shown in Fig. 6(a)–(c) and 6(d)–(f), metric and topological rules show a non-monotonic dependence on threshold size in most cases. This may occur since certain moderate scales (e.g., $R_{\text{metr}} = 7 \text{ m}$ and $\eta_{\text{topo}} = 40\%$) generate multiple mesoscale clusters, whose subsequent competition and consolidation amplify small stochastic asymmetries into a dominant flow and maximize the degree of imbalance. Conversely, small scales are too weakly coupled to coordinate across clusters, preventing large-scale directional alignment, while large scales impose near-global coupling that quickly aligns the majority preferences, smoothing out intermediate competitive

effects. However, visual rules do not exhibit this phenomenon, because even at maximum visibility ($\theta_{\text{vis}} = 0.00 \text{ rad}$) in Fig. 5(g)–(i), occlusions limit the number of effectively perceived neighbors and prevent unrealistic near-global coupling. The intrinsic constraint endows visual neighborhoods with robust adaptivity to capture realistic, density-geometry dependent decision dynamics, in line with VR-based experimental evidence supporting the visually driven interaction hypothesis in human crowds [38].

Turning now to Fig. 7, we explore how the leaving time for 90% people depends on interaction neighborhoods under different panic and density levels. At low density in Fig. 7(a), (d), and (g), most cases show that the leaving time drops with increasing p_i at first and then levels off or rises slightly, with optima appearing at larger panic ($p_i = 0.6 \sim 0.9$). This reflects that, in sparse crowds, exit exploration dominates evacuation time, while stronger herding accelerates information contagion and directional consensus toward exits. Across all interaction networks, the overall leaving time is minimized at relatively small neighborhood scales ($R_{\text{metr}} = 3 \text{ m}$, $\eta_{\text{topo}} = 10\%$, and $\theta_{\text{vis}} = 0.20 \text{ rad}$), perhaps this setting balances independent exploration with information sharing. Both excessively small and large neighborhoods increase evacuation time, by respectively slowing exit information spread or inducing premature collective alignment that concentrates flow. As density increases in Fig. 7(b)–(c), (e)–(f), and (h)–(i), the vast majority of optima shift toward intermediate panic ($p_i = 0.3 \sim 0.7$) at medium density and smaller panic ($p_i = 0.1 \sim 0.4$) at high density. This arises because denser crowds are prone to excessive herding and severe exit congestion, thus weaker panic preserves more individualistic searching that helps alleviate

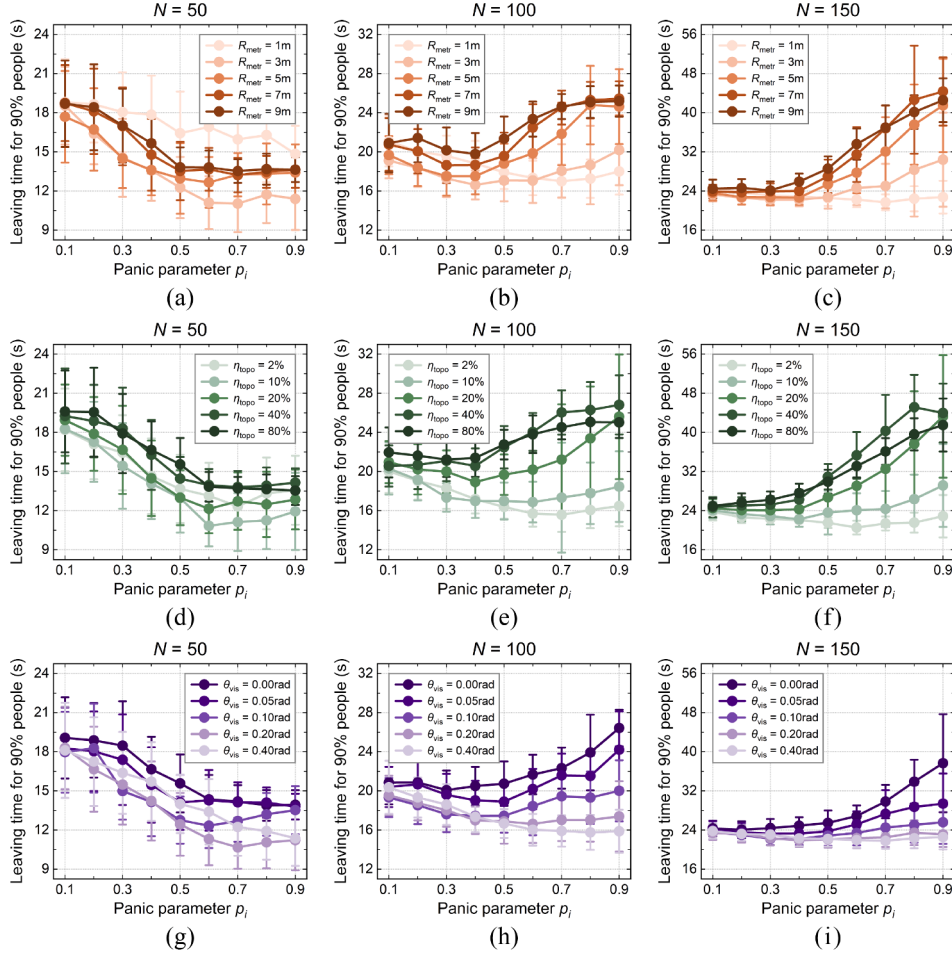


Fig. 7. Effect of interaction neighborhoods on the leaving time for 90 % people under different panic and density levels. (a)–(c) Metric network. (d)–(f) Topological network. (g)–(i) Visual network. The solid circle and error bar represent the mean value and standard deviation in 50 trials, respectively.

overload bottlenecks. Notably, for metric and topological networks, the leaving time also varies non-monotonically with increasing threshold, with the longest time occurring at moderate scales, where intermittent congestion driven by mesoscale clusters maximizes evacuation delays. In contrast, visual networks display a strictly monotonic rise of leaving time as θ_{vis} shrinks, since occlusions prevent extremely large coupling even at maximum visibility, and thus the effective interaction scale may not reach the level that would produce the longest delays. Moreover, at high density, visual rules typically yield lower exit usage asymmetry in Fig. 6(i) and shorter leaving times in Fig. 7(i) than metric or topological cases, because visual constraints preserve more heterogeneous choices, thereby mitigating extreme congestion around exits.

3.4. Optimal regimes of decision-making rationality for efficient evacuation

The primary concern for crowd evacuation is efficiency. Here, the panic parameter p_i actually reflects the relative degree of herding versus individualistic decision-making (i.e., deviation from fully rational behavior). This section focuses on the leaving time under different conditions to identify optimal regimes of decision-making rationality for efficient evacuation. As behavior shifts from near-individualistic ($p_i = 0.1 \sim 0.3$), through mixed ($p_i = 0.4 \sim 0.6$), toward near-herding ($p_i = 0.7 \sim 0.9$), variations in environmental constraints (density level) and individual perception (neighborhood scale) may influence leaving time differently. To characterize this diversity, we systematically vary the initial number of people N to span density levels from sparse to dense, and adjust network thresholds R_{metr} , η_{topo} , θ_{vis} to create neighborhood scales

from small to large. Across all interaction networks in Fig. 8, a common pattern is that increasing p_i amplifies disparities in the leaving time under different density levels and neighborhood scales. In other words, evacuation efficiency becomes more polarized: under favorable conditions stronger herding accelerates collective coordination and shortens leaving time, but under unfavorable ones it reinforces congestion and leads to much longer delays. This growing polarization reflects the intensification effect of herding behavior. When p_i is low, individuals retain autonomy in decision-making and the leaving time is only weakly affected by density level or neighborhood scale, whereas stronger p_i enforces alignment with neighbors and amplifies the influences of environmental constraints and individual perception. As a result, higher p_i magnifies the sensitivity of evacuation efficiency to initial settings, thereby producing more significant heterogeneity across different conditions. Notably, this exacerbation of the polarization effect is less significant in visual networks, because visual neighborhoods are inherently governed by angular perception, which restricts extreme congestion caused by large-scale synchronization and suppresses the upward amplification of efficiency polarization.

For each panel in Fig. 8, increasing density naturally prolongs the leaving time across all interaction neighborhoods, while this metric shows distinct sensitivities to neighborhood scales. Specifically, in Fig. 8(a), (d), and (g), when people remain near-individualistic ($p_i = 0.1 \sim 0.3$), the threshold corresponding to the minimum leaving time stays almost within a stable range regardless of density. This stability arises because in relatively rational regimes, decisions are dominated by individual goals and only weakly integrate social cues from

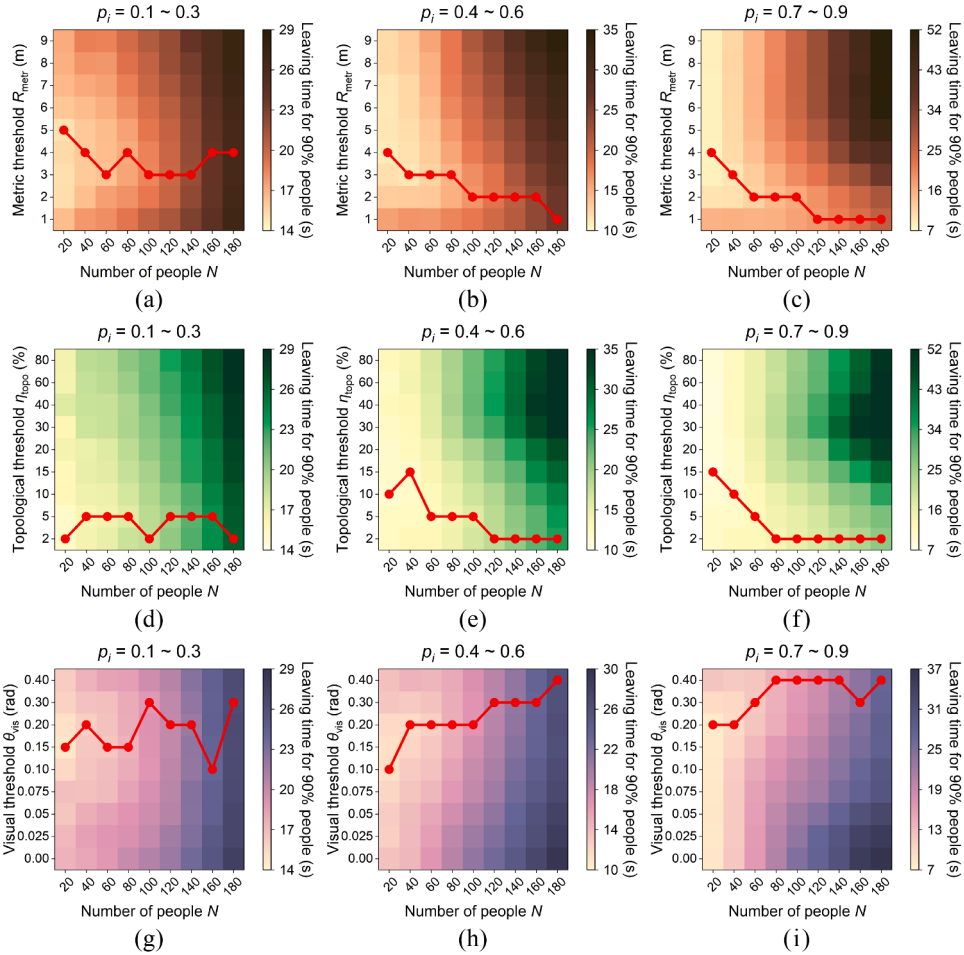


Fig. 8. Effects of density levels and neighborhood scales on the leaving time for 90 % people under different panic levels. (a)–(c) Metric network. (d)–(f) Topological network. (g)–(i) Visual network. The color coding of the square corresponds to mean value in 50 trials, and the red dotted line reflects the threshold corresponding to the minimum leaving time at each density level.

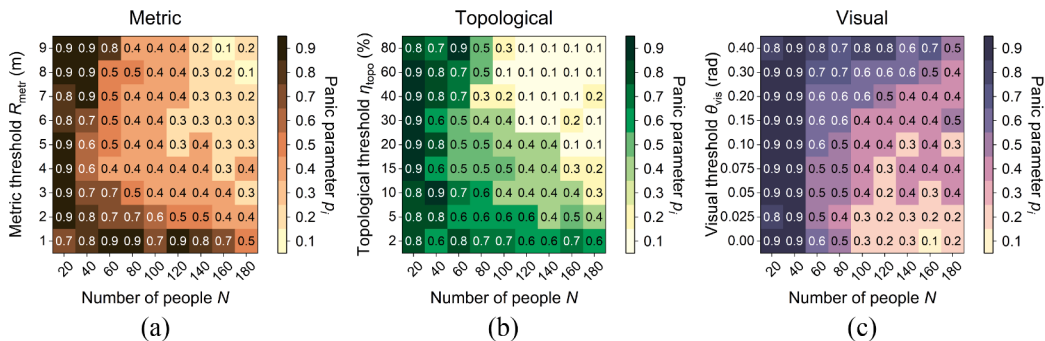


Fig. 9. Panic parameter p_i corresponding to the minimum leaving time for 90 % people under different density levels and neighborhood scales. (a) Metric network. (b) Topological network. (c) Visual network. The number in the square represents the optimal value obtained from the mean value in 50 trials.

neighbors. Hence, raising density merely adds potential neighbors without increasing their influence, leaving optimal thresholds mainly determined by perceptual constraints rather than by density levels. For metric networks the optimum lies around $R_{\text{metr}} = 3 \sim 5 \text{ m}$, for topological networks it remains about $\eta_{\text{topo}} = 2 \sim 5 \%$, while for visual networks it falls within $\theta_{\text{vis}} = 0.10 \sim 0.30 \text{ rad}$. The difference among the three cases reflects their unique definitions: spatial distance for metric, nearest-neighbor amount for topological, and angular perception for visual. As p_i strengthens in Fig. 8(b)–(c), (e)–(f), and (h)–(i), individual states become mixed ($p_i = 0.4 \sim 0.6$) or near-herding ($p_i = 0.7 \sim 0.9$). With the growth

of density, the optimal thresholds for metric and topological networks gradually shift downward, while those for visual networks move upward, which consistently indicates that smaller neighborhood scales are preferable. This is because in denser and stronger herding crowds, considering too many neighbors promotes excessive synchronization and long-range correlation, which reinforces blockage formation, whereas restricting interactions to fewer close neighbors can preserve a degree of local variability and facilitate smoother flow. In summary, this convergence implies that when panic dominates decision-making, the fastest evacuation efficiency (i.e., minimum leaving time) is governed more by

density levels and neighborhood scales, rather than by the specific definition of interaction neighborhoods.

Furthermore, as visualized in Fig. 9, we determine the panic parameter p_i corresponding to the minimum leaving time for 90 % people under different density levels and neighborhood scales. In sparse settings or with small interaction ranges, larger p_i leads to faster evacuation efficiency, meaning that stronger herding behavior is beneficial. In such cases, individuals gain from quickly aligning with others, which accelerates information spreading and helps reduce exploratory wandering in under-informed environments. Conversely, under dense conditions with large interaction ranges, smaller p_i facilitates collective escape, i.e., individuals should behave more individualistically. Excessive herding in such crowded situations easily amplifies congestion near exits, while a greater degree of independence helps to distribute flows more evenly and alleviate crowd congestion. In other cases, intermediate p_i is the optimal regime that balances autonomy and conformity, where individualism enables partial people to find available exits and herding ensures that correct choices can be followed by others. Although metric, topological, and visual rules differ in how they define interaction neighborhoods, the resulting patterns in Fig. 9(a)–(c) are remarkably similar. These results indicate that the optimal regimes, reflecting specific trade-offs between individualistic and herding behavior, depend on the combined effects of density levels and neighborhood scales.

4. Conclusions

In this work, we utilize a social force model of escape panic to compare how interaction neighborhoods, defined by metric, topological, or visual networks, affect crowd behavior in panic evacuation. Through a series of numerical simulations, several key conclusions are summarized as follows: (1) All three neighborhood definitions can reproduce behavioral transitions from individualistic to herding under panic conditions, but they differ in shaping individual decisions and collective outcomes. (2) Each interaction rule governs the proportion of effective neighbors in a characteristic way, and larger neighborhood scales generally amplify exit usage asymmetry and slow evacuation efficiency. (3) The occlusion-induced constraint endows visual neighborhoods with robust adaptivity, preventing threshold artifacts observed in metric and topological cases and capturing realistic, density-geometry dependent decision dynamics. (4) At higher panic, leaving time becomes more polarized across density levels and neighborhood scales, and its minimum value remains largely independent of neighborhood definitions. (5) Optimal regimes of decision-making rationality for efficient evacuation are provided: stronger herding in sparse or small-neighborhood cases, greater individualism in dense and large-neighborhood ones, and intermediate strategy otherwise.

This study functions as a methodological guide for selecting interaction neighborhood rules in evacuation simulations based on the escape-panic social force framework. Our results indicate that neighborhood assumptions can substantially influence exit usage asymmetry and evacuation efficiency, especially under variable-density conditions. If the research focus is on capturing fine-grained collective dynamics within a wide range of densities and geometries, visual neighborhoods, owing to intrinsic occlusion constraints, are methodologically superior and can reduce sensitivity to threshold selection. In contrast, for applications where density is relatively controlled and computational simplicity is prioritized, metric or topological neighborhoods may provide efficient approximations. The flexibility allows us to balance methodological fidelity with computational efficiency depending on specific research objectives. This work also offers conceptual suggestions for building evacuation in various environments (e.g., density, visibility, and layout), particularly with respect to directional choices at room exits or corridor junctions. While real-world panic itself cannot be directly controlled, our model identifies optimal regimes of decision-making rationality that maximize evacuation efficiency within the framework. As higher panic has been widely associated with less rationality in most studies [39],

interventions can be designed to affect how evacuees make decisions, thereby indirectly guiding crowds toward these regimes. Interventions that promote individualism, such as adding visible exit signage or audible exit information, can support autonomous and rational choices. In contrast, strategies that facilitate herding, such as deploying voice broadcasts (e.g., calls for walking in groups [42]) or evacuation guides, can strengthen cohesion and conformity behavior.

Furthermore, this study has several limitations that define the scope of its applicability and point toward future research directions. First, our work is framed as a methodological comparison of interaction neighborhood definitions and does not include empirical validation of human behavioral mechanisms. While this approach allows us to systematically evaluate how different modeling choices affect simulation outcomes, the conclusions regarding actual crowd behavior should be interpreted with caution. Second, the model assumes instantaneous responses to neighbors, which is a simplifying abstraction that omits learning, adaptation, or feedback mechanisms. This may overestimate collective responsiveness and interaction strength, and therefore cannot capture staged responses [43] or behavioral contagion processes [44] during emergency evacuation. Third, homogeneous human crowds are adopted, with identical physical and behavioral parameters. While this controlled setting allows us to isolate the effects of interaction neighborhoods, the model is not able to predict variability arising from individual differences in physical capacity, psychological states, or risk sensitivity [45,46]. Last, the environment is assumed to be static, and feedback mechanisms between pedestrian behavior and environmental conditions (e.g., smoke spread [47] or dynamically changing hazards) are not considered. It is hard for this model to account for coupled human-environment dynamics or adaptive route choices driven by evolving conditions. Therefore, future work will likely require integrating interaction neighborhood models with adaptive behavioral rules, heterogeneous individual features, and dynamically evolving environments, potentially informed by empirical data or evidence. Notwithstanding these limitations, this study underscores the critical role of neighborhood definitions in the computational modeling of collective human behavior and offers a comparative framework that assists modelers in selecting appropriate interaction rules, thereby improving the reliability and interpretability of crowd evacuation simulations.

CRediT authorship contribution statement

Wenhan Wu: Writing – review & editing, Writing – original draft, Visualization, Validation, Software, Methodology, Investigation, Formal analysis, Conceptualization; **Wenfeng Yi:** Writing – review & editing, Writing – original draft, Validation, Supervision, Software, Resources, Project administration, Methodology, Investigation, Funding acquisition.

Data availability

Data will be made available on request.

Declaration of competing interest

The authors declare that they have no known competing financial interests or personal relationships that could have appeared to influence the work reported in this paper.

Acknowledgment

This work was supported by the National Natural Science Foundation of China (No. 62506386).

References

- [1] Feliciani C, Corbett A, Haghani M, Nishinari K. Trends in crowd accidents based on an analysis of press reports. *Saf Sci* 2023;164:106174. <https://doi.org/10.1016/j.ssci.2023.106174>

- [2] Duan J, Liu H, Fan B, Li X, Li W. Evacuation under terrorist attacks: a crowd control method based on deep reinforcement learning. *Reliab Eng Syst Saf* 2026;267:111951. <https://doi.org/10.1016/j.ress.2025.111951>
- [3] Haghani M, Sarvi M. Crowd behaviour and motion: empirical methods. *Transp Res Part B Methodol* 2018;107:253–94. <https://doi.org/10.1016/j.trb.2017.06.017>
- [4] Haghani M, Yazdani M. How simple behavioural modifications can influence evacuation efficiency of crowds: part 1. Decision making of individuals. *Transp Res Part C Emerging Technol* 2024;166:104763. <https://doi.org/10.1016/j.trc.2024.104763>
- [5] Haghani M, Yazdani M. How simple behavioural modifications can influence evacuation efficiency of crowds: part 2. Physical movement of individuals. *Transp Res Part C Emerging Technol* 2024;166:104762. <https://doi.org/10.1016/j.trc.2024.104762>
- [6] Zheng X, Zhong T, Liu M. Modeling crowd evacuation of a building based on seven methodological approaches. *Build Environ* 2009;44(3):437–45. <https://doi.org/10.1016/j.buildenv.2008.04.002>
- [7] Yi W, Wu W. Control strategies for order-disorder phase transition in crowd evacuation. *Reliab Eng Syst Saf* 2026;266:111688. <https://doi.org/10.1016/j.ress.2025.111688>
- [8] Aldahlawi RY, Akbari V, Lawson G. A systematic review of methodologies for human behavior modelling and routing optimization in large-scale evacuation planning. *Int J Disaster Risk Reduct* 2024;110:104638. <https://doi.org/10.1016/j.ijdrr.2024.104638>
- [9] He Z, Shen K, Lan M, Weng W. The effects of dynamic multi-hazard risk assessment on evacuation strategies in chemical accidents. *Reliab Eng Syst Saf* 2024;246:110044. <https://doi.org/10.1016/j.ress.2024.110044>
- [10] Raafat RM, Chater N, Frith C. Herding in humans. *Trends Cogn Sci* 2009;13(10):420–8. <https://doi.org/10.1016/j.tics.2009.08.002>
- [11] Haghani M, Sarvi M. Imitative (herd) behaviour in direction decision-making hinders efficiency of crowd evacuation processes. *Saf Sci* 2019;114:49–60. <https://doi.org/10.1016/j.ssci.2018.12.026>
- [12] Li Y, Mao Q, Li Y, Zuo M, Wan X. An evacuation model considering multi-attribute group decision-making behavior. *Reliab Eng Syst Saf* 2026;268:111976. <https://doi.org/10.1016/j.ress.2025.111976>
- [13] Moussaïd M, Kapadia M, Thrash T, Sumner RW, Gross M, Helbing D, et al. Crowd behaviour during high-stress evacuations in an immersive virtual environment. *J R Soc Interface* 2016;13(122):20160414. <https://doi.org/10.1098/rsif.2016.0414>
- [14] Ni M, Xia L, Li C, Wei Y, Deng F, Liu Z, et al. Herd behavior influence on decision-making during evacuation process: an empirical analysis from building evacuation experiments. *Curr Psychol* 2024;43(43):33390–405. <https://doi.org/10.1007/s12144-024-06806-8>
- [15] Chen A, He J, Liang M, Su G. Crowd response considering herd effect and exit familiarity under emergent occasions: a case study of an evacuation drill experiment. *Physica A* 2020;556:124654. <https://doi.org/10.1016/j.physa.2020.124654>
- [16] Fu M, Liu R, Zhang Y. Do people follow neighbors? an immersive virtual reality experimental study of social influence on individual risky decisions during evacuations. *Autom Constr* 2021;126:103644. <https://doi.org/10.1016/j.autcon.2021.103644>
- [17] Lin J, Zhu R, Li N, Becerik-Gerber B. Do people follow the crowd in building emergency evacuation? A cross-cultural immersive virtual reality-based study. *Adv Eng Inf* 2020;43:101040. <https://doi.org/10.1016/j.aei.2020.101040>
- [18] Liu Y, Mao Z. An experimental study on the critical state of herd behavior in decision-making of the crowd evacuation. *Physica A* 2022;595:127087. <https://doi.org/10.1016/j.physa.2022.127087>
- [19] Van den Berg M, van Nes R, Hoogendoorn S. Estimating choice models to quantify the effect of herding on the decision to evacuate: application of a serious gaming experimental setup. *Transp Res Rec J Transp Res Board* 2018;2672(1):161–70. <https://doi.org/10.1177/0361198118784404>
- [20] Haghani M, Sarvi M. 'Herding' in direction choice-making during collective escape of crowds: how likely is it and what moderates it? *Saf Sci* 2019;115:362–75. <https://doi.org/10.1016/j.ssci.2019.02.034>
- [21] Lovreglio R, Borri D, dell'Olio L, Ibeas A. A discrete choice model based on random utilities for exit choice in emergency evacuations. *Saf Sci* 2014;62:418–26. <https://doi.org/10.1016/j.ssci.2013.10.004>
- [22] Lovreglio R, Fonzone A, dell'Olio L, Borri D. A study of herding behaviour in exit choice during emergencies based on random utility theory. *Saf Sci* 2016;82:421–31. <https://doi.org/10.1016/j.ssci.2015.10.015>
- [23] Wang J, Chen M, Yan W, Zhi Y, Wang Z. A utility threshold model of herding-panic behavior in evacuation under emergencies based on complex network theory. *Simulation* 2016;93(2):123–33. <https://doi.org/10.1177/0037549716678659>
- [24] Helbing D, Farkas I, Vicsek T. Simulating dynamical features of escape panic. *Nature* 2000;407(6803):487–90. <https://doi.org/10.1038/35035023>
- [25] Yuan Z, Jia H, Zhang L, Bian L. A social force evacuation model considering the effect of emergency signs. *Simulation* 2017;94(8):723–37. <https://doi.org/10.1177/0037549717741350>
- [26] Meng Q, Zhou M, Liu J, Dong H. Pedestrian evacuation with herding behavior in the view-limited condition. *IEEE Trans Comput Social Syst* 2019;6(3):567–75. <https://doi.org/10.1109/tcss.2019.2915772>
- [27] Tan J, Zhang W, Nong T, Zhang Z, Wang T, Ma Y, et al. An improved social force model based on nucleus force theory to simulate building evacuation in different visibility conditions. *Simul Model Pract Theory* 2025;142:103117. <https://doi.org/10.1016/j.simpat.2025.103117>
- [28] Poel W, Winklmayr C, Romanczuk P. Spatial structure and information transfer in visual networks. *Front Phys* 2021;9. <https://doi.org/10.3389/fphy.2021.716576>
- [29] Couzin ID, Krause J, Franks NR, Levin SA. Effective leadership and decision-making in animal groups on the move. *Nature* 2005;433(7025):513–16. <https://doi.org/10.1038/nature03236>
- [30] Evangelista DJ, Ray DD, Raja SK, Hedrick TL. Three-dimensional trajectories and network analyses of group behaviour within chimney swift flocks during approaches to the roost. *Proc R Soc B Biol Sci* 2017;284(1849):20162602. <https://doi.org/10.1098/rspb.2016.2602>
- [31] Rio KW, Dachner GC, Warren WH. Local interactions underlying collective motion in human crowds. *Proc R Soc B Biol Sci* 2018;285(1878):20180611. <https://doi.org/10.1098/rspb.2018.0611>
- [32] Ballerini M, Cabibbo N, Candelier R, Cavagna A, Cisbani E, Giardina I, et al. Interaction ruling animal collective behavior depends on topological rather than metric distance: evidence from a field study. *Proc Natl Acad Sci* 2008;105(4):1232–7. <https://doi.org/10.1073/pnas.0711437105>
- [33] Camperi M, Cavagna A, Giardina I, Parisi G, Silvestri E. Spatially balanced topological interaction grants optimal cohesion in flocking models. *Interface Focus* 2012;2(6):715–25. <https://doi.org/10.1098/rsfs.2012.0026>
- [34] Jayles B, Escobedo R, Pasqua R, Zanon C, Blanchet A, Roy M, et al. Collective information processing in human phase separation. *Phil Trans R Soc B Biol Sci* 2020;375(1807):20190801. <https://doi.org/10.1098/rstb.2019.0801>
- [35] Bastien R, Romanczuk P. A model of collective behavior based purely on vision. *Sci Adv* 2020;6(6). <https://doi.org/10.1126/sciadv.aaq0792>
- [36] Lemasson BH, Anderson JJ, Goodwin RA. Collective motion in animal groups from a neurobiological perspective: the adaptive benefits of dynamic sensory loads and selective attention. *J Theor Biol* 2009;261(4):501–10. <https://doi.org/10.1016/j.jtbi.2009.08.013>
- [37] Strandburg-Peshkin A, Twomey CR, Bode N WF, Kao AB, Katz Y, Ioannou CC, et al. Visual sensory networks and effective information transfer in animal groups. *Curr Biol* 2013;23(17):R709–R711. <https://doi.org/10.1016/j.cub.2013.07.059>
- [38] Wirth TD, Dachner GC, Rio KW, Warren WH. Is the neighborhood of interaction in human crowds metric, topological, or visual? *PNAS Nexus* 2023;2(5). <https://doi.org/10.1093/pnasnexus/pgad118>
- [39] Haghani M, Cristiani E, Bode N WF, Boltes M, Corbetta A. Panic, irrationality, and herding: three ambiguous terms in crowd dynamics research. *J Adv Transp* 2019;2019:1–58. <https://doi.org/10.1155/2019/9267643>
- [40] Ji Q, Xin C, Tang SX, Huang JP. Symmetry associated with symmetry break: revisiting ants and humans escaping from multiple-exit rooms. *Physica A* 2018;492:941–7. <https://doi.org/10.1016/j.physa.2017.11.024>
- [41] Sun Kim C, Dib C, Oh S. Spontaneous symmetry breaking and panic escape. *PLoS ONE* 2025;20(5):e0322862. <https://doi.org/10.1371/journal.pone.0322862>
- [42] Wu W, Yi W, Wang X, Zheng X. A vision-driven model based on cognitive heuristics for simulating subgroup behaviors during evacuation. *IEEE Trans Intell Transp Syst* 2024;25(11):16048–58. <https://doi.org/10.1109/tits.2024.3421626>
- [43] Rosenthal SB, Twomey CR, Hartnett AT, Wu HS, Couzin ID. Revealing the hidden networks of interaction in mobile animal groups allows prediction of complex behavioral contagion. *Proc Natl Acad Sci* 2015;112(15):4690–5. <https://doi.org/10.1073/pnas.1420068112>
- [44] Wu W, Yi W. Modeling the dynamical process of behavioral contagion in human crowds during evacuation. *Reliab Eng Syst Saf* 2026;266:111649. <https://doi.org/10.1016/j.ress.2025.111649>
- [45] Wu W, Chen M, Li J, Liu B, Zheng X. An extended social force model via pedestrian heterogeneity affecting the self-driven force. *IEEE Trans Intell Transp Syst* 2022;23(7):7974–86. <https://doi.org/10.1109/tits.2021.3074914>
- [46] Wu W, Li J, Yi W, Zheng X. Modeling crowd evacuation via behavioral heterogeneity-based social force model. *IEEE Trans Intell Transp Syst* 2022;23(9):15476–86. <https://doi.org/10.1109/tits.2022.3140823>
- [47] Richardson O, Jalba A, Muntean A. Effects of environment knowledge in evacuation scenarios involving fire and smoke: a multiscale modelling and simulation approach. *Fire Technol* 2018;55(2):415–36. <https://doi.org/10.1007/s10694-018-0743-x>